Bioprinting 16 (2019) e00059

Contents lists available at ScienceDirect

Bioprinting

journal homepage: www.elsevier.com/locate/bprint

In vivo remodeling of a 3D-Bioprinted tissue engineered heart valve scaffold

Eva L. Maxson [1], Melissa D. Young [1], Christopher Noble, Jason L. Go, Behnam Heidari, Reza Khorramirouz, David W. Morse, Amir Lerman [*]

Department of Cardiovascular Medicine, Mayo Clinic, Rochester, MN, USA

ARTICLE INFO

Keywords:
Bioprinting
Tissue engineering
Collage-based matrix
Mechanical behavior
Heart valve

ABSTRACT

Objective: To evaluate the recellularization potential of a bioprinted aortic heart valve scaffold printed with highly concentrated Type I collagen hydrogel (Lifeink® 200) and MSCs.

Materials and methods: A suspension of rat mesenchymal stem cells (MSCs) was mixed with Lifeink® 200 and was 3D-printed into gelatin support gel to produce disk scaffolds which were subsequently implanted subcutaneously in Sprague-Dawley rats for 2, 4, 8, and 12 weeks. The biomechanical properties of the scaffolds were evaluated by uniaxial tensile testing and cell infiltration and inflammation assessed via immunohistochemistry (IHC) and histological staining.

Results: There was an average decrease in both UTS and tensile modulus from 2 to 4 weeks followed by an increase between 4 to 8 weeks and a plateau from 8 to 12 weeks. IHC showed a continued expression of alpha smooth muscle actin and vimentin biomarkers throughout the study demonstrating continued presence of interstitial-like and fibroblast-like cells. Additionally, there was also an increase of elastin at each time point.

Conclusion: The profile of the stress-strain curves of the bioprinted aortic heart valve scaffolds indicated that the scaffold transitioned through phases of resorption, synthesis, stabilization, and ultimately, remodeling. This is supported by IHC and histology which showed favorable remodeling capacity demonstrating potential feasibility for a 3D printed heart valve.

1. Introduction

According to the American Heart Association, there have been approximately 600,000 deaths due to valvular heart disease (VHD) since 1979 [1,2]. Currently, the gold standard for aortic valve disease (AVD) is limited to either mechanical or bioprosthetic valve replacement. Mechanical valves require anticoagulation and are typically applied to younger patients, while bioprosthetic valves have limited durability and are prone to calcific degradation [3]. Tissue engineered heart valves (TEHV) have become increasingly important in the development of valve replacement because of availability and customizability for individual patients. Although TEHV have limitations such as antigenicity and loss of extracellular matrix integrity to overcome, there is significant promise showing autologous host cell remodeling of these scaffolds [4]. Three-dimensional (3D) bioprinting has become popular and increasingly used in medicine to produce biomaterials ready for implantation. The technology has applications that allow for living cells to be printed within a synthetic scaffold that presents in a variety of shapes, complexities, and mechanical properties [5]. In recent years, the medical industry has increasingly used 3D-printing to create patient-specific prosthetics, surgical models, and drug delivery devices [6]. Unlike biological tissue, bioprinting allows for the artificial creation of organs and tissues for on-demand manufacturing with patient cells [7].

3D-bioprinting allows for host cell integration coupled with ECM remodeling to establish a viable TEHV that will grow and adapt with the patient. This technology can achieve homogenous porosity and allow deposition of different cell types within a construct [8]. 3D-bioprinted valves are customizable to patients though direct digital input from patient imaging utilizing computed tomography and ultrasound imaging. The precise spatial control has the capability to print complex native valvular structures with autologous cells. 3D-bioprinting has been used to construct a heterogeneous aortic valve structure, using different materials for the root and the leaflets. More recently, the technique has been used to build a model of an aortic valve leaflet, giving each different layer specific mechanical properties [9,10]. 3D-bioprinting enables reproducibility that cannot be replicated with biological tissue scaffolds [11].

* Corresponding author. 200 First St SW, Rochester, MN, 55905, USA.
E-mail address: lerman.amir@mayo.edu (A. Lerman).
[1] Contributed equally to this work.

https://doi.org/10.1016/j.bprint.2019.e00059
Received 27 February 2019; Received in revised form 12 August 2019; Accepted 14 August 2019

The biomaterial selected to produce a scaffold must have the proper biocompatibility and degradation rate that will allow for structure maintenance, cellular maturity, and enable active cellular remodeling. Additionally, the material requires mechanical integrity and stability throughout the printing process in order to prevent layer collapse. Consideration of cell type and environmental conditioning is necessary to strengthen the valve to endure hemodynamic pressures. Potential mechanisms for crosslinking such as UV light or chemical crosslinking maybe considered to strengthen the scaffold and allow for the structure to maintain shape during environmental conditioning [12]. Thus, a novel approach should be developed to constructing the 3D biological heart valve.

The focus of the current manuscript is to evaluate the collagen-based bio-ink biocompatibility and its recellularization potential for use as a heart valve implant. This study involves a hybrid approach for 3D printing and *in vivo* biomaterial characterization of the collagen-based bio-ink via rat subcutaneous evaluation.

2. Materials and Methods

2.1. Specimen preparation

A computer aided design model (CAD) for the implant disk scaffolds was created utilizing Solidworks (Dassault Systèmes, Waltham, MA) and Magics Materialise 3D rendering software (Materialise n.v. 2011, Magic EnvisionTec 32 bit V16.2.0.20). CAD model files were exported to Perfactory software (EnvisionTec v 3.2.2945), converted to stereolithography (.STL) files, and uploaded to the 3D-bioplotter control software Visual Machines (version 2.8.129r1).

2.1.1. FRESH preparation

Freeform Reversible Embedding of Suspended Hydrogels (FRESH) slurry was made under aseptic conditions according to previously published methods [13]. FRESH slurry was dispensed into 50 mL Falcon tubes. Centrifugation was performed and supernatant removed and replaced with DMEM. Tubes were shaken to homogenize the DMEM with resuspended gelatin particles. This was repeated several times to remove insoluble gelatin and to incorporate the cell culture medium into the FRESH slurry. The DMEM-FRESH slurry was dispensed into a 6-well plate.

2.1.2. Cell culture and bio-ink preparation

Allogenic rat mesenchymal stem cells (rMSCs) labelled with green fluorescent protein (GFP) (Cyagen Biosciences Inc., Santa Clara, CA) were cultured at 37 °C in 5% CO_2 in Dulbecco's modified Eagle's Medium (DMEM, Gibco, Life Technologies). This was supplemented with 5% heat-inactivated fetal bovine serum (FBS, Atlas Biologicals) and 1% antibiotic-antimycotic (A/A, Gibco) until the number of necessary cells was reached. Media was changed every two days. Cultured cells, passaged at 80% confluence, were washed 3 times using phosphate buffer saline (PBS), detached from the culture vessel with Trypsin-EDTA (Gibco Life Technologies), suspended in DMEM, and centrifuged at 1800 RPM. The supernatant was removed and cells were counted and resuspended to achieve a concentration of 6×10^6 cells/mL of Bio-ink (5:2 ratio of Lifeink® 200: cell media) per manufacturer's protocol. The cell suspension was loaded into a 5 mL syringe and attached to the tip of a 10 mL syringe containing Lifeink® 200® using a lumen connector. Lifeink® 200 and the cell suspension were mixed until a homogenous Bio-ink was achieved. The cell-laden Bio-ink was loaded into a syringe (EFD Nordson) compatible with the EnvisionTEC 3D-Bioplotter (EnvisionTEC GmbH, Gladbeck, Germany).

2.1.3. 3D-printing of the implant disk scaffolds

The CAD model for the implant disk scaffolds measured 1 mm-thick and 28 mm-diameter was sliced into a 0.1 mm thickness, and uploaded to Visual Machines. This geometry was utilized as it could be easily implanted in the rat subcutaneous space and easily mounted in the support frame which prevented migration and folding. A more physiologically relevant shape could not be easily implanted in the subcutaneous space and likely would not have a large impact on the recellularization or remodeling as the biological and physical cues would not have been greatly altered. One disk scaffold was printed per well-plate. The inner diameter of the needle to extrude the Bio-Ink was 0.1 mm and 25 mm in length. The needle transfer height was 35 mm, needle offset was 0.1 mm, and printing speed and pressure were 14 mm/s and 1.6 bar, respectively. The temperature of the printing platform and the printing head were set at 4 °C and 23 °C, respectively. Disk scaffolds were printed in a layer-by-layer fashion, each layer printed in a continuous manner with a 0.3 mm distance between individual extruded strands and a 90° offset between the strand orientation in each layer. The description of the strands here is applicable during the printing process; during cross-linking, the individual strands fuse together. Pre-flow and post-flow delays were set at 200 ms and 100 ms, respectively. After the printing process, well-plates were placed in a 37 °C, 5% CO_2 environment for 45–60 min. The liquefied gelatin was subsequently removed and the Bio-ink disk scaffolds were cultured for 5 days in DMEM with 1% A/A and 5% FBS. Under aseptic conditions, the cultured Bio-ink disk scaffolds were placed between polycaprolactone (PCL) support frames. Vetbond (3 M, Maplewood, MN) surgical glue was used to fix both PCL frames together with the disk scaffolds in the middle [14]. In our previous study we investigated the effect of a PCL support frame on tissue remodeling in the rat subcutaneous space with decellularized pericardium. We found superior remodeling and fewer propensities for tissue folding or migration with the PCL support frames and so utilized this approach in this work [14].

2.2. Collagen- based bio-ink biomaterial characterization

2.2.1. In vivo performance

Twelve Sprague Dawley rats were obtained and raised in a pathogen-free environment. In vivo assessment of the scaffolds was conducted at 2, 4, 8, and 12 weeks (each rat had $n = 4$ implants, for a total of $n = 48$ and $n = 12$ for each time point). All experiments were performed in strict accordance with the guidelines in the Guide for Institutional Animal Care and Use Committee (IACUC protocol number: A00003286-17). The surgical procedure and the PCL support frames (Fig. 1A) used to house the Bio-ink disk scaffolds were 3D-printed following the same method described in previous studies [14]. Explanted disk scaffolds were divided for 1) mechanical testing, and 2) fixed in 10%Formalin and preserved in 70% EtOH for immunohistochemistry.

2.2.2. Immunohistochemistry, immunofluorescence, and histology

Bioprinted implant disk scaffolds were paraffin-embedded then sectioned at the Mayo Clinic Pathology Core (Scottsdale, AZ). Immunohistochemistry (IHC) methodology can be found in previous publications [4,14]. Primary antibodies were used to express recellularization, extracellular matrix remodeling, and immune reaction of the bioprinted explant. Primary antibodies utilized were CD163 (Abcam, Cambridge, UK) and CD3 (Abcam) for immune reaction, Vimentin (Abcam) and Alpha smooth muscle Actin (Abcam) for interstitial-like cell phenotypes, CD31 (Abbiotec, San Diego, CA) for endothelialization, Elastin (Abcam) for elastic tissue, and Collagen I (Thermofisher) for Collagen Type 1. Images were quantitatively analyzed in terms of antibody signal surface area using ImageJ software and a digital slide scanner (MoticEasyScan, Motic). Immunofluorescence (IF) was performed to visualize the green fluorescent protein (GFP)-positive cells preseeded on the bioprinted acellular implant disk scaffolds. Sections were incubated with the primary antibody rabbit polyclonal to GFP (ThermoFisher, Waltham, MA) overnight at room temperature. The stain was labelled using a secondary antibody donkey anti-rabbit IgG H&L Alexa Fluor 488 (Thermofisher) mounted using Prolong Gold Anti-Fade Mountant with DAPI (Thermofisher), and visualized with a confocal microscope. Additionally, samples

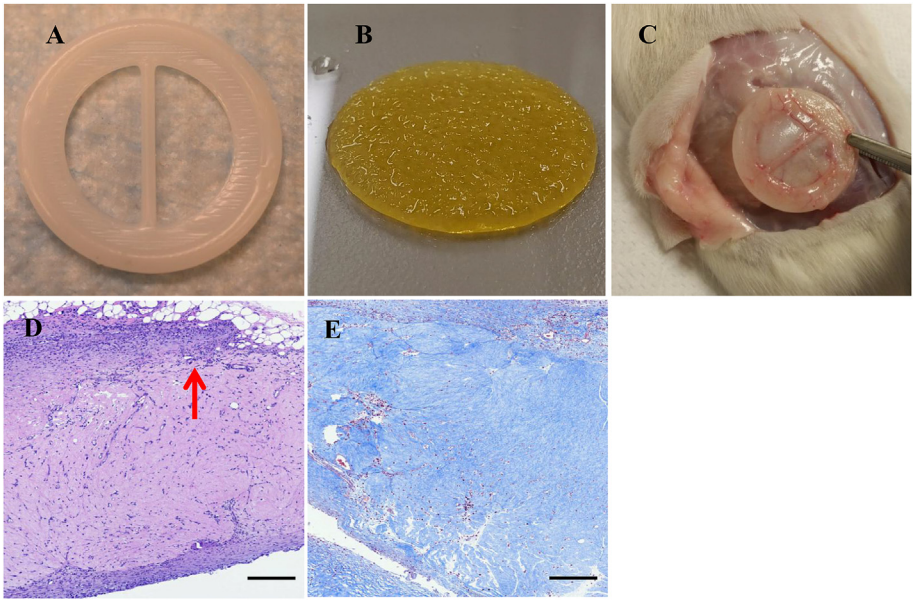

Fig. 1. Top view images showing (A) half the PCL support frame, and (B) the bioprinted sample. The 3D-printed heart valve scaffold (C) explanted at 12 weeks *in vivo*. Immunohistochemistry staining of explanted scaffold (D) Hematoxylin and eosin (H&E) visualized using a Motic EasyScan slidescanner, scale = 300 μm. There was an observed increase in host cellular concentration found at the periphery (red arrow) and infiltrating within the 3D bioprinted disk scaffold.(E) Masson's trichrome, scale = 300 μm shows a diffuse blue expression representative of collagen within the 3D bioprinted disk scaffold. (For interpretation of the references to colour in this figure legend, the reader is referred to the Web version of this article.)

were stained with Hematoxylin-Eosin (H&E), Masson Trichromeand elastin stains to observe cellularity, collagen depositionand fibrosis; respectively.

2.3. Mechanical performance

The mechanical properties of the explanted bioprinted scaffold were assessed by conducting uniaxial tensile testing per ASTM F2150-13 (n = 12 per time point 2, 4, 8, 12 weeks). The tensile testing was performed using a tensile tester (Instron, USA, Series 5900). Each sample was cut with a constant width of 4 mm and varying length. The thickness was measured with a drop gauge (Mitutoyo America Corp., Aurora, IL, USA). The samples were placed within the grips of the machine, and the specimen gauge length was measured and recorded. The samples were stretched until failure, which occurred midway between the grips, using a displacement rate of 0.16667 mm/s. The load as a function of the extension data was recorded and processed using MATLAB and Statistics Toolbox Release R2016a (The MathWorks Inc., Natick, Massachusetts). The ultimate tensile strength was computed as being the maximal value on the stress-strain curve, and the tensile modulus was computed as being the slope in the linear region on the stress-strain curve.

2.3.1. Statistical analysis

Data distribution was analyzed utilizing MATLAB statistics toolbox using a one way ANOVA followed by a multi-comparison test. Data is presented as mean ± SD with statistical significance defined as P value < 0.05. Furthermore, to determine if there was a relationship between the tissue stiffness and the quantified concentrations of the IHC parameters linear regression analysis was performed across all time points with the R^2 value reported to indicate goodness-of-fit.

3. Results

3.1. Collagen-based bioink in-vivo biomaterial characterization

All animals (n = 12) survived the implantation procedure without any clinical evidence of wound infection or inflammation. Prior to implantation, the Bioink implants were observed to be fragile; however, after each time point, the physical handling of each explant had improved. After four weeks, the Bioink explants contained a fibrous capsule with neovascularization. Additionally, it was observed that layers of the host tissue had integrated with the Bioink explant, and after eight weeks, both layers had become indistinguishable (Fig. 1). Despite this integration, the structural integrity of the extracellular matrix remained intact with cellularization of host cells on the Bioink explant. Fibrosis was prevalent on the cutaneous side of the Bioink explant as seen with Masson's trichrome (Fig. 1).

For immunohistochemistry, immunofluorescence and histology, semi-quantification was done utilizing the surface area of the tissue and expression of specific biomarkers. Chronic inflammation and ECM remodeling were observed with the biomarkers CD3 and CD163 (Fig. 2). The linear regression analysis found that no IHC parameters had strong correlation with the tissue stiffness (Table 1). The highest R^2 value was for vimentin (0.277) and the lowest for collagen (0.002).

3.1.1. Weeks 2–4 post-implantation

There was a decreased expression of CD3 as observed from the cross-sectional surface area of explanted Bioink tissue from week 2 (2.47 ± 0.5) to week 4 (1.16 ± 0.09) due to a reduced presence of chronic inflammatory cells ($p = 0.002$). There was a decrease in CD163 expression from week 2 (2.55 ± 0.24) to week 4 (2.15 ± 0.21). From week 2 (1.36 ± 0.17) to week 4 (3.43 ± 0.58), there was a statistically significant increase in the expression of the CD31 biomarker for endothelialization and angiogenesis between the host tissue and Bioink explant ($p < 0.05$) (Fig. 3). Alpha smooth muscle actin and vimentin biomarkers revealed an increase of interstitial-like cells infiltrating the Bioink explants over time (Fig. 4). At weeks 2 and 4, there was an increased concentration of vimentin in the surrounding tissue (Week 2: 3.84 ± 1.12; Week 4: 5.49 ± 0.31). There was also an increase in presence of elastin during this time period. From a mechanical property standpoint; stress versus strain plots from tensile testing are shown in Fig. 5. Between 2 and 4 weeks, the strength of the mean sample decreases. The UTS and tensile modulus are given in Fig. 6 as mean ± standard deviation. One-way analysis of variance (ANOVA) was run. The values for UTS were 0.344 ± 0.120 and 0.169 ± 0.077 MPa for 2 and 4 weeks, respectively, showing a decrease over time. The same statistical analysis was run for the tensile modulus, which was taken to be the slope of the stress-strain curve. There was a decrease in the tensile modulus from 2 to 4 weeks (1.186 ± 0.872 and 0.548 ± 0.341 MPa, respectively).

3.1.2. Weeks 4–8 post-implantation

There was a decrease in CD163 expression from week 4 (2.15 ± 0.21) to week 8 (1.74 ± 0.14) (Fig. 2). Overall, there was a steady decrease of CD163 expression from week 1 (2.55 ± 0.24) to week 8 (1.74 ± 0.14;

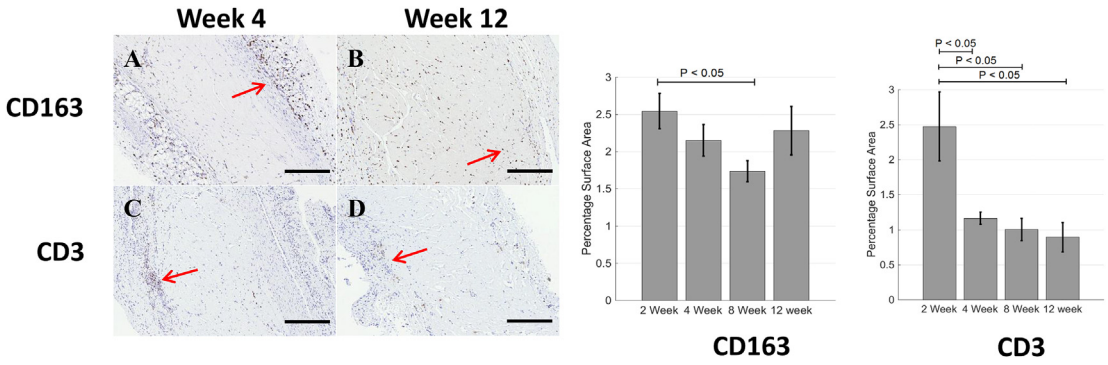

Fig. 2. (A–D) CD163 and CD3 immunohistochemistry staining for heart valve scaffold printed with rMSCs, visualized using a Motic EasyScan slidescanner, at 4 and 12 weeks, scale = 300 μm. Red arrows show expression of CD163 and CD3 biomarkers that are used to determine inflammation and type II macrophages. Week 4 shows expression along the disk scaffold periphery while at the end of the study, type 2 macrophages where observed to be interspersed throughout the disk scaffold. The graphs to the right show CD163 and CD3 quantifications at 2, 4, 8, and 12 weeks where significance ($P < 0.05$) is displayed. (For interpretation of the references to colour in this figure legend, the reader is referred to the Web version of this article.)

Table 1
Slope and R^2 value from a linear regression analysis of the quantified IHC with the tensile modulus.

	CD 163	CD 3	CD 31	Elastin	Vimentin	α SMA
Slope	−0.181	−0.069	−0.222	0.2383	1.238	0.126
R^2	0.122	0.005	0.036	0.010	0.277	0.022

$p < 0.05$) reflecting a decrease in inflammation. At week 4, the expression of CD31 biomarker started to taper (Week 4: 3.43 ± 0.58; Week 8: 2.56 ± 0.25). During this time period, the elastin presence continued to increase, and the largest increase of elastin occurred between week 2 (3.74 ± 0.62 and week 8 (7.12 ± 1.13) ($p = 0.03$). The stress-strain plots show a change in shape in the general curve and a visible increase in strength from 4 to 8 weeks. There was an increase in the UTS from 4 to 8 weeks (0.275 ± 0.166 MPa). There was also a statistically significant

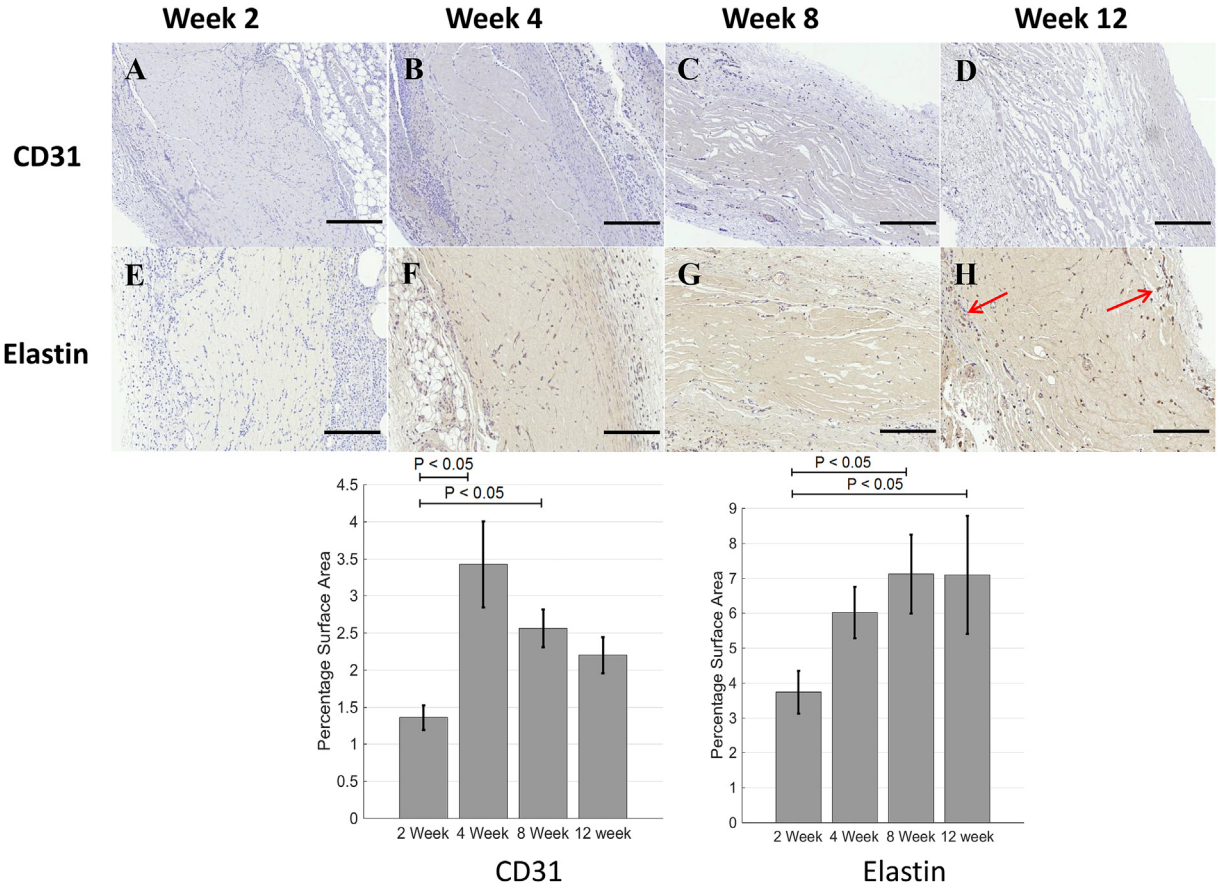

Fig. 3. (A–D) CD31 staining of the heart valve scaffold explants at 2, 4, 8 and 12 weeks, scale bars = 300 μm. Red Arrows show expression of the CD31 biomarker for cellular endothelialization. (E–H) Elastin staining of the heart valve scaffold explants at 2, 4, 8 and 12 weeks, scale bars = 300 μm. Red Arrows show expression of the elastin biomarker for elastin composition in the 3D bioprinted tissue. Statistical representations of CD31 and Elastin quantifications at 2, 4, 8, and 12 weeks are shown in the graphs below, where significance ($P < 0.05$) is displayed. (For interpretation of the references to colour in this figure legend, the reader is referred to the Web version of this article.)

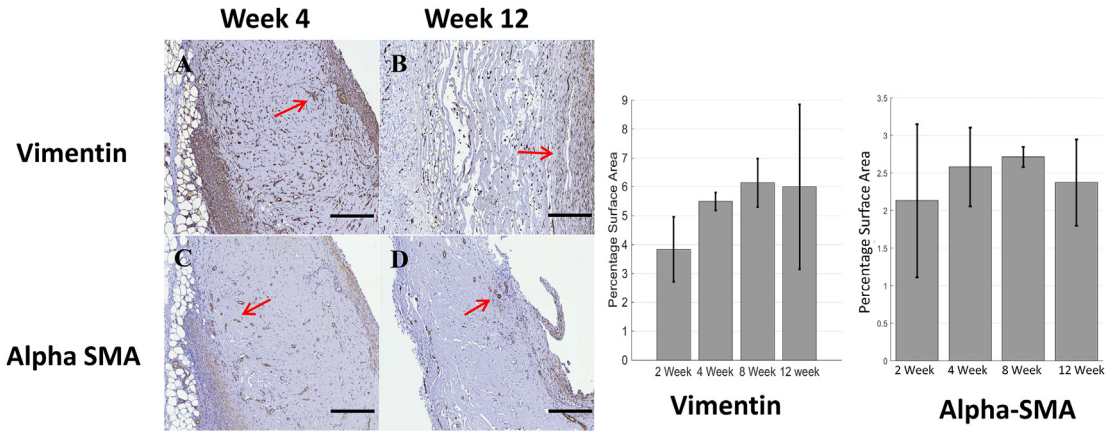

Fig. 4. Vimentin staining of the heart valve scaffold at (A) week 4 and (B) week 12. Alpha SMA staining at (C) week 4 and (D) week 12, scale bars = 300 μm. Red arrows show expression of vimentin and α-SMA biomarkers that are used to determine interstitial-like and myofibroblast-like cells that are found in active tissue remodeling. Graphical representation of Vimentin and Alpha SMA expression throughout the *in vivo* study. (For interpretation of the references to colour in this figure legend, the reader is referred to the Web version of this article.)

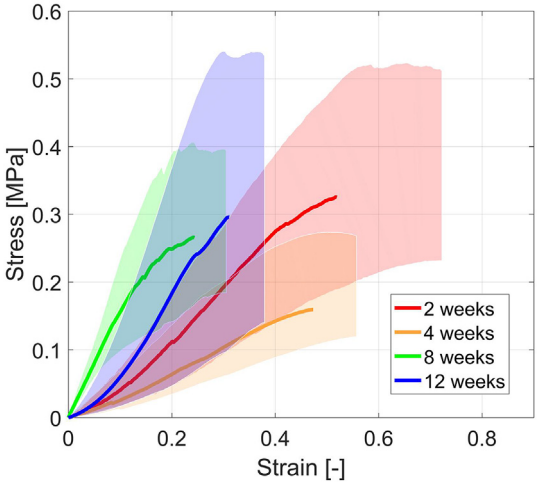

Fig. 5. Stress versus strain plot of the heart valve scaffolds at 2, 4, 8, and 12 weeks. The solid line demonstrates the mean and the transparent regions the variability of the data. The mechanical property evolution demonstrates the vast transition of the tissue engineered scaffold as it undergoes resorption, synthesis, stabilization, and remodeling phases.

increase in the tensile modulus from 0.548 ± 0.341 to 1.425 ± 0.620 MPa ($p < 0.05$).

3.1.3. *Weeks 8–12 post implantation*

There was an increase in CD163 expression from week 8 (1.74 ± 0.14) to week 12 (2.28 ± 0.32) due to subsequent infiltration of M2 macrophages (Fig. 2). The expression of CD31 biomarker continued to decrease (Week 8: 2.56 ± 0.25, Week 12: 2.20 ± 0.25) and fibrotic tissue started to encapsulate the Bioink explant by week 12. After week 8, vimentin concentration within the Bioink explant increased (Week 8; 6.14 ± 0.85) ($p = 0.05$) (Fig. 4). From 8 to 12 weeks, there is a decrease in strength again, along with a change in the shape of the plot curve, which returns to more of a shape similar to 2 and 4 week samples but with lower strain at fracture. The UTS was 0.306 ± 0.176 MPa at 12 weeks, showing an increase between 8 weeks and 12 weeks. There was a very slight decrease in the tensile modulus from 1.425 ± 0.620 to 1.376 ± 0.616 MPa. The increase of the tensile modulus from 4 to 12 weeks was computed to be of statistical significance ($p < 0.05$).

4. Discussion

The current study demonstrated that 12 week rat subcutaneous implantations revealed the pathway to remodeling for this scaffold that included resorption, synthesis, stabilization, and remodeling phases. The

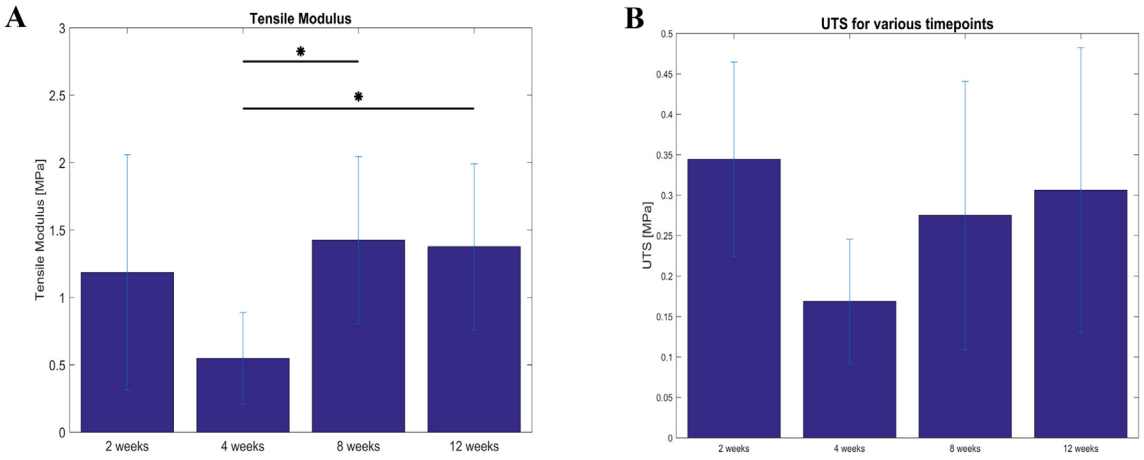

Fig. 6. Mechanical property analysis for heart valve scaffold with the (A) Tensile modulus after 2, 4, 8 and 12 weeks and (B) Ultimate tensile strength after 2, 4, 8 and 12 weeks, where * denotes significance ($P < 0.05$).

in vivo studies showed increased host cellularization potential, biocompatibility, and biomechanical behavior results. The bio-ink was successfully printed with MSCs and showed remodeling. Thus, the current study supports the potential use of a collagen-based bio-ink as an alternative for a tissue engineered heart valve implant.

Throughout the *in vivo* study, the bioprinted implant scaffolds went through a remodeling pathway characterized by 1) resorption, 2) synthesis, 3) stabilization, and 4) remodeling. These stages were critical for the tissue engineered scaffold to be strengthened over time. The resorption stage, where the host environment integrates the scaffold and partially degrades it, is seen by the initial drop in the tensile modulus and UTS for the scaffold from week 2 to week 4. During this time, there was an initial increase in CD3 biomarker from acute inflammation. In similar studies, degradation and resorption responses in tissue engineered scaffolds made from porcine pericardial tissue and small intestinal submucosa were also observed [13–16]. The synthesis stage, where the host tissue begins infiltrating the scaffold, found an increase in UTS and tensile modulus from week 4 to week 8. When evaluating CD31a biomarker for angiogenesis and endothelialization, there was a significant increase from week 2 to week 4. However, upon explantation the scaffold had gross encapsulation from the host tissue and signs of neovascularization.

The stabilizing stage occurred between weeks 8 and 12. The inflammation leveled out as shown by the decreased CD3 biomarker expression. At this point; elastin, vimentin, and alpha SMA production were at its peak as observed by immunohistochemistry staining, which indicated that the infiltrated cells were actively depositing collagen and strengthening the extracellular matrix in the bioprinted scaffold. Both the UTS and the tensile modulus peaked and plateaued, which indicated a biomechanical equilibrium for the scaffold. The final stage and perhaps the most important was classified as a period of remodeling and occurred starting at week 12. This stage was detected microscopically as well as through the IHC straining results where the CD31 biomarker for angiogenesis was at its maximum at week 12. The CD163 biomarker for M2 macrophages showed a steady increasing trend, and was at its greatest at week 12 suggesting good regenerative capacity over time. Biomechanical evaluation showed that both tensile modulus and UTS increased significantly from week 4 to week 12. The UTS and tensile modulus are comparable to findings previously published with fibrin-based gel to engineer a pediatric heart valve [17].

In addition to the results from the rat subcutaneous implantation, we were able to successfully print a heart valve utilizing the same bio-ink from the *in vivo* study with MSCs. Obtaining valve structure is a complex balance of processes and materials. The bio-ink material must allow cells to infiltrate, support itself during the printing process, and achieve cell survival throughout the extrusion process. Researchers are exploring new material combinations to obtain cell viability. Some materials investigated include, but are not limited to alginate, agarose, collagen, gelatin, hyaluronic acid (HA), decellularized tissue and polycaprolactone, polyethylene glycol (PEG) [9,18–23]. Duan et al. 3D-bioprinted a living alginate/gelatin hydrogel valve using smooth muscle cells and valvular interstitial cells, which showed viability *in vitro* for 7 days [9].

Similar mechanical behavior to the remodeling phase seen in this work can be identified in reverse for tissues with elastin removed by enzymatic digestion. The change in mechanical response between 12 and 8 weeks is similar to arterial tissues where elastin has been removed [24–26]. Collagen, held in a crimped configuration, is released and so is immediately stretched giving an immediate stiff response rather than there being an initial toe region where the elastin is stretched and the collagen unfurled. This coincides with our theory of tissue remodeling where we speculate that the synthesized components are being reorganized such that collagen is being crimped to give the two stage mechanical response common for soft tissues.

The bioprinted heart valve scaffolds have much lower strength compared to native aortic valve cusps, where native valve cusps have an average UTS of 2.6 and 0.4 MPa in the circumferential and radial directions, respectively [27]. Therefore, preconditioning will be of utmost importance, slowly increasing the pressures applied to the scaffold until physiological pressures are met and the scaffold can strengthen [6–8,11]. Potentially after preconditioning, if the scaffold is strong enough before implantation the resorption phase will be smaller or may not occur at all. There have also been various cross-linking methods used to increase mechanical strength of the bioprinted structures post-printing, but most of them involve a process that is cytotoxic [5]. Future steps will involve using visible-light crosslinking with ruthenium and sodium persulfate prior to valve preconditioning to achieve greater mechanical stability [28–30].

Outside of valvular applications, current technologies that have been explored include the work by Yu et al. where spheroid technology was utilized to create tissue strands by printing alginate micro-conduits. They synthesized cell tissue strands that were formed up to 4 days post-fabrication with viability close to 90% [31]. For application in the nervous system, Gu et al. constructed neural tissue by printing neural stem cells using alginate, carboxylmethyl-chitosan, and agarose bio-ink [18]. While, Lee et al. 3D-bioprinted collagen bio-ink, reinforced with polycaprolactone, with 3 types of cells to construct artificial liver tissue where a co-culture of the cells was maintained over time [19]. Skardal et al. also 3D-bioprinted primary liver spheroids with a modular HA and gelatin-based hydrogel and showed high cell viability [20]. Lee et al. used PCL and a cell-laden hydrogel to 3D-bioprint an ear and showed chondrogenesis and adipogenesis through *in vitro* assays [23]. Finally for printing of generic scaffolds, Ouyang et al. studied a dual-cross-linking hyaluronic acid system that enabled them to achieve structures that were stable for over a month [32]. While Pati et al. were able to 3D-bioprint with decellularized extracellular matrix material showing high cell viability and functionality [33]. These studies provide insight to the challenges of obtaining shape, geometry, and function of the printed construct while maintaining cell viability.

One limitation is that the cells used for the bioprinted scaffolds were commercially bought, and not from the actual implanted rats. This could be the cause of some of the inflammatory reaction and would need to be further assessed. Additionally, this study did not evaluate the influence of the presence of the PCL scaffolds on the remodeling process. PCL has been shown to be biocompatible and to induce minimal inflammatory responses [34]. Additionally, the implantation time was too short to expect any type of degradation of the PCL, as PCL has been shown to have long degradation times, exceeding the timeframe of this study [35,36]. An aspect that must be studied further is the effect of the remaining FRESH gelatin in the Bio-Ink lattice, after cross-linking. However, we do not expect this to have a negative effect. As mentioned in Ref. [37], gelatin is biocompatible, and may actually enhance cell adhesion and integration with the bioprinted scaffold [38].

The rat subcutaneous space does not provide the same mechanical cues as the physiological valve environment. However, there are obvious difficulties in performing large animal studies in sufficient numbers to provide statistical power to the results. The goal of this study was to evaluate the collagen-based bio-ink biocompatibility and its recellularization potential for use as a heart valve implant. From this, the bioprinting approach can be refined prior to more costly and exhaustive larger animal studies wherein the final optimized approach can be ascertained from a reduced number of possible designs. Our previous study utilized a similar approach with decellularized-sterilized porcine pericardium to similarly evaluate the recellularization and remodeling potential and performed subsequent finite element analyses to evaluate the performance as a TEHV prior to large animal studies [39]. For this work, the good association between the mechanical performance, histology, and IHC of the 12 week explants and the native tissues lends confidence to the current scaffold structure for this purpose and going forward.

Finally, the fibrous capsule was not investigated in this study. It is known that this is a key indicator to the host response to the implanted

tissue including internal cellularization and differentiation [40–42]. However, we lacked the sample size to analyze this independently and thus this must be considered a limitation of this work.

5. Conclusion

We evaluated a 3D printed collagen based bio-ink tissue engineered heart valve scaffold. *In vivo* studies proved the scaffold had favorable remodeling capacity with increasing elastin, vimentin, alpha SMA, and CD31 throughout the 12 weeks. The pathway for remodeling stages included resorption, synthesis, stabilization, and remodeling. Each phase played a key role to improve strength and mechanical stability over time. Additionally, the current study introduced a 3D bioprinted scaffold that contains rMSCs that would assist in recellularization. The addition of rMSCs to the 3D scaffold attracted host cells to repopulate the scaffold, which further strengthened the synthetic ECM architecture. We hypothesized that seeded rMSCs encouraged host cell recellularization behavior. An aortic heart valve was 3D printed with MSCs and sustained a valve shape. The results show great promise in the use of a collagen-based bioink for heart valve construction using 3D-bioprinting technology.

Support

This work is supported by the HH Sheikh Hamed bin Zayed Al Nahyan Program in Biological Valve Engineering. In addition, this research was supported in part by a National Institutes of Health T32 (HL007111) training grant in Cardiovasology.

Competing interest

The author(s) declare no competing interests.

Acknowledgments

The authors would like to acknowledge Darrell Loeffler and Lisa Nesbitt for their assistance with this project. The authors would also like to acknowledge Advanced Biomatrix for their help in optimizing the protocols for the use of Lifeink® 200 in our studies. This work is supported by the HH Sheikh Hamed bin Zayed Al Nahyan Program in Biological Valve Engineering. In addition, this research was supported in part by a National Institutes of Health T32 training grant in Cardiovasology (HL007111 to JG). The authors confirm that there are no known conflicts of interest associated with this publication and there has been no significant financial support for this work that could have influenced its outcome.

Appendix A. Supplementary data

Supplementary data to this article can be found online at https://doi.org/10.1016/j.bprint.2019.e00059.

Author contribution statement

Author Eva Maxson conducted the bioprinting studies, wrote the rough draft, and performed the literature search. Melissa Young was responsible for the initial study design, IACUC protocol, data analysis, supervision of the laboratory tests, and manuscript writing and editing. Jason Go contributed to manuscript writing and editing and IHC analysis. Christopher Noble performed mechanical properties analysis and statistical analysis. Behnam Heidari and Reza Khorramirouz performed the *in vivo* surgeries. David Morse prepared specimens, assisted with surgical studies, conducted mechanical testing and IHC staining. Amir Lerman edited the manuscript, contributed to the clinical insight of the paper, and supervised activities of the study.

References

[1] R.O. Bonow, A.S. Brown, L.D. Gillam, S.R. Kapadia, C.J. Kavinsky, B.R. Lindman, M.J. Mack, V.H. Thourani, G.J. Dehmer, R.O. Bonow, B.R. Lindman, T.M. Beaver, S.M. Bradley, B.A. Carabello, M.Y. Desai, I. George, P. Green, D.R. Holmes Jr., D. Johnston, J. Leipsic, S.L. Mick, J.J. Passeri, R.N. Piana, N. Reichek, C.E. Ruiz, C.C. Taub, J.D. Thomas, Z.G. Turi, J.U. Doherty, G.J. Dehmer, S.R. Bailey, N.M. Bhave, A.S. Brown, S.L. Daugherty, L.S. Dean, M.Y. Desai, C.S. Duvernoy, L.D. Gillam, R.C. Hendel, C.M. Kramer, B.D. Lindsay, W.J. Manning, P. Mehrotra, M.R. Patel, R. Sachdeva, L.S. Wann, D.E. Winchester, J.M. Allen, ACC/AATS/AHA/ASE/EACTS/HVS/SCA/SCAI/SCCT/SCMR/STS 2017 appropriate use criteria for the treatment of patients with severe aortic stenosis: a report of the American college of cardiology appropriate use criteria task force, American association for thoracic surgery, American heart association, American society of echocardiography, european association for cardio-thoracic surgery, heart valve society, society of cardiovascular anesthesiologists, society for cardiovascular angiography and interventions, society of cardiovascular computed tomography, society for cardiovascular magnetic resonance, and society of thoracic surgeons, J. Am. Soc. Echocardiogr. : Off. Publ. Am. Soc. Echocardiogr. 31 (2) (2018) 117–147.
[2] A.S. Go, M.A. Bauman, S.M. Coleman King, G.C. Fonarow, W. Lawrence, K.A. Williams, E. Sanchez, An effective approach to high blood pressure control: a science advisory from the American Heart Association, the American College of Cardiology, and the Centers for Disease Control and Prevention, J. Am. Coll. Cardiol. 63 (12) (2014) 1230–1238.
[3] I. Vesely, Heart valve tissue engineering, Circ. Res. 97 (8) (2005) 743–755.
[4] R.S. Hennessy, J.L. Go, R.R. Hennessy, B.J. Tefft, S. Jana, N.J. Stoyles, M.A. Al-Hijji, J.J. Thaden, S.V. Pislaru, R.D. Simari, J.M. Stulak, M.D. Young, A. Lerman, Recellularization of a novel off-the-shelf valve following xenogenic implantation into the right ventricular outflow tract, PLoS One 12 (8) (2017), e0181614.
[5] S.V. Murphy, A. Atala, 3D bioprinting of tissues and organs, Nat. Biotechnol. 32 (2014) 773.
[6] C.L. Ventola, Medical applications for 3D printing: current and projected uses, PT : Peer-Rev. J. Formul. Manage. 39 (10) (2014) 704–711.
[7] U. Jammalamadaka, K. Tappa, Recent advances in biomaterials for 3D printing and tissue engineering, J. Funct. Biomater. 9 (1) (2018).
[8] S. Stratton, O.S. Manoukian, R. Patel, A. Wentworth, S. Rudraiah, S.G. Kumbar, Polymeric 3D printed structures for soft-tissue engineering, J. Appl. Polym. Sci. 135 (24) (2018).
[9] B. Duan, L.A. Hockaday, K.H. Kang, J.T. Butcher, 3D bioprinting of heterogeneous aortic valve conduits with alginate/gelatin hydrogels, J. Biomed. Mater. Res. A 101 (5) (2013) 1255–1264.
[10] D.C. van der Valk, C.F.T. van der Ven, M.C. Blaser, J.M. Grolman, P.J. Wu, O.S. Fenton, L.H. Lee, M.W. Tibbitt, J.L. Andresen, J.R. Wen, A.H. Ha, F. Buffolo, A. van Mil, C.V.C. Bouten, S.C. Body, D.J. Mooney, J.P.G. Sluijter, M. Aikawa, J. Hjortnaes, R. Langer, E. Aikawa, Engineering a 3d-bioprinted model of human heart valve disease using nanoindentation-based biomechanics, Nanomaterials 8 (5) (2018) (Basel, Switzerland).
[11] J. An, J.E.M. Teoh, R. Suntornnond, C.K. Chua, Design and 3D printing of scaffolds and tissues, Engineering 1 (2) (2015) 261–268.
[12] W. Jia, P.S. Gungor-Ozkerim, Y.S. Zhang, K. Yue, K. Zhu, W. Liu, Q. Pi, B. Byambaa, M.R. Dokmeci, S.R. Shin, A. Khademhosseini, Direct 3D bioprinting of perfusable vascular constructs using a blend bioink, Biomaterials 106 (2016) 58–68.
[13] T.J. Hinton, Q. Jallerat, R.N. Palchesko, J.H. Park, M.S. Grodzicki, H.J. Shue, M.H. Ramadan, A.R. Hudson, A.W. Feinberg, Three-dimensional printing of complex biological structures by freeform reversible embedding of suspended hydrogels, Sci. Adv. 1 (9) (2015), e1500758.
[14] R. Khorramirouz, J.L. Go, C. Noble, S. Jana, E. Maxson, A. Lerman, M.D. Young, A novel surgical technique for a rat subcutaneous implantation of a tissue engineered scaffold, Acta Histochem. 120 (3) (2018) 282–291.
[15] S.F. Badylak, B. Kropp, T. McPherson, H. Liang, P.W. Snyder, Small intestinal submucosa: a rapidly resorbed bioscaffold for augmentation cystoplasty in a dog model, Tissue Eng. 4 (4) (1998) 379–387.
[16] R.G. Khorramirouz, J.L, C. Noble, D. Morse, A. Lerman, M.D. Young, In Vivo Response of Acellular Porcine Pericardial for Tissue Engineered Transcatheter Aortic Valves, Scientific Reports, 2018 (In Submission).
[17] C.J. Tefft BJ, M.D. Young, R.S. Hennessy, D.W. Morse, J.A. Bouchard, H.J. Hedberg, J.F. Consiglio, D. Dragomir-Daescu, R.D. Simari, Lerman A Cardiac Valve Bioreactor for Physiological Conditioning and Hydrodynamic Performance Assessment, Cardiovascular Engineering and Technology, 2018.
[18] Q. Gu, E. Tomaskovic-Crook, R. Lozano, Y. Chen, R.M. Kapsa, Q. Zhou, G.G. Wallace, J.M. Crook, Functional 3D neural mini-tissues from printed gel-based bioink and human neural stem cells, Adv. Healthc. Mater. 5 (12) (2016) 1429–1438.
[19] J.W. Lee, Y.J. Choi, W.J. Yong, F. Pati, J.H. Shim, K.S. Kang, I.H. Kang, J. Park, D.W. Cho, Development of a 3D cell printed construct considering angiogenesis for liver tissue engineering, Biofabrication 8 (1) (2016), 015007.
[20] A. Skardal, M. Devarasetty, H.W. Kang, I. Mead, C. Bishop, T. Shupe, S.J. Lee, J. Jackson, J. Yoo, S. Soker, A. Atala, A hydrogel bioink toolkit for mimicking native tissue biochemical and mechanical properties in bioprinted tissue constructs, Acta Biomater. 25 (2015) 24–34.
[21] L. Ouyang, C.B. Highley, C.B. Rodell, W. Sun, J.A. Burdick, 3D printing of shear-thinning hyaluronic acid hydrogels with secondary cross-linking, ACS Biomater. Sci. Eng. 2 (10) (2016) 1743–1751.
[22] F. Pati, J. Jang, D.H. Ha, S. Won Kim, J.W. Rhie, J.H. Shim, D.H. Kim, D.W. Cho, Printing three-dimensional tissue analogues with decellularized extracellular matrix bioink, Nat. Commun. 5 (2014) 3935.

[23] J.S. Lee, J.M. Hong, J.W. Jung, J.H. Shim, J.H. Oh, D.W. Cho, 3D printing of composite tissue with complex shape applied to ear regeneration, Biofabrication 6 (2) (2014), 024103.
[24] A.Y. Lee, B. Han, S.D. Lamm, C.A. Fierro, H.-C. Han, Effects of elastin degradation and surrounding matrix support on artery stability, Am. J. Physiol. Heart Circ. Physiol. 302 (2012) H873–H884.
[25] M.-J. Chow, J.R. Mondonedo, V.M. Johnson, Y. Zhang, Progressive structural and biomechanical changes in elastin degraded aorta, Biomechanics Model. Mechanobiol. 12 (2013) 361–372.
[26] S. Zeinali-Davarani, M.-J. Chow, R. Turcotte, Y. Zhang, Characterization of biaxial mechanical behavior of porcine aorta under gradual elastin degradation, Ann. Biomed. Eng. 41 (2013) 1528–1538.
[27] A. Balguid, M.P. Rubbens, A. Mol, R.A. Bank, A.J. Bogers, J.P. van Kats, B.A. de Mol, F.P. Baaijens, C.V. Bouten, The role of collagen cross-links in biomechanical behavior of human aortic heart valve leaflets–relevance for tissue engineering, Tissue Eng. 13 (7) (2007) 1501–1511.
[28] Z.H. Syedain, J. Bjork, L. Sando, R.T. Tranquillo, Controlled compaction with ruthenium-catalyzed photochemical cross-linking of fibrin-based engineered connective tissue, Biomaterials 30 (35) (2009) 6695–6701.
[29] K.S. Lim, B.S. Schon, N.V. Mekhileri, G.C.J. Brown, C.M. Chia, S. Prabakar, G.J. Hooper, T.B.F. Woodfield, New visible-light photoinitiating system for improved print fidelity in gelatin-based bioinks, ACS Biomater. Sci. Eng. 2 (10) (2016) 1752–1762.
[30] J.W. Bjork, S.L. Johnson, R.T. Tranquillo, Ruthenium-catalyzed photo cross-linking of fibrin-based engineered tissue, Biomaterials 32 (10) (2011) 2479–2488.
[31] Y. Yu, I.T. Ozbolat, Tissue strands as "bioink" for scale-up organ printing, Conference proceedings :, in: ... Annual International Conference of the IEEE Engineering in Medicine and Biology Society. IEEE Engineering in Medicine and Biology Society. Annual Conference 2014, 2014, pp. 1428–1431.
[32] C. Loebel, C.B. Rodell, M.H. Chen, J.A. Burdick, Shear-thinning and self-healing hydrogels as injectable therapeutics and for 3D-printing, Nat. Protoc. 12 (8) (2017) 1521–1541.
[33] F. Pati, D.W. Cho, Bioprinting of 3D tissue models using decellularized extracellular matrix bioink, Methods Mol. Biol. 1612 (2017) 381–390 (Clifton, N.J.).
[34] K.M. Ainslie, S.L. Tao, K.C. Popat, H. Daniels, V. Hardev, C.A. Grimes, T.A. Desai, In vitro inflammatory response of nanostructured titania, silicon oxide, and polycaprolactone, J. Biomed. Mater. Res. A 91A (3) (2009) 647–655.
[35] M. Thiel, P.C. Rodrigues Palma, C.L.Z. Riccetto, M. Dambros, N.R. Netto Jr., A stereological analysis of fibrosis and inflammatory reaction induced by four different synthetic slings, BJU Int. 95 (6) (2005) 833–837.
[36] H. Sun, L. Mei, C. Song, X. Cui, P. Wang, The in vivo degradation, absorption and excretion of PCL-based implant, Biomaterials 27 (9) (2006) 1735–1740.
[37] J.M. Dang, K.W. Leong, Natural polymers for gene delivery and tissue engineering, Adv. Drug Deliv. Rev. 58 (4) (2006) 487–499.
[38] J.-S. Chun, M.-J. Ha, B.S. Jacobson, Differential translocation of protein kinase C ε during HeLa cell adhesion to a gelatin substratum, J. Biol. Chem. 271 (22) (1996) 13008–13012.
[39] C. Noble, J. Choe, S. Uthamaraj, M. Deherrera, A. Lerman, M. Young, In silico performance of a recellularized tissue-engineered transcatheter aortic valve, J. Biomech. Eng. 141 (2019), 061004.
[40] B.D. Ratner, Healing with medical implants: the body battles back, Sci. Transl. Med. 7 (2015) 7–10.
[41] E.M. Sussman, M.C. Halpin, J. Muster, R.T. Moon, B.D. Ratner, Porous implants modulate healing and induce shifts in local macrophage polarization in the foreign body reaction, Ann. Biomed. Eng. 42 (7) (2014) 1508–1516.
[42] L. Zhang, Z. Cao, T. Bai, L. Carr, J.-R. Ella-Menye, C. Irvin, B.D. Ratner, S. Jiang, Zwitterionic hydrogels implanted in mice resist the foreign-body reaction, Nat. Biotechnol. 31 (2013) 553.